Supplementary Information for:

Tracking amyloid oligomerization with monomer resolution using a 13-amino acid peptide with a backbone-fixed spin label

E. Zurlo[a], I. Gorroño Bikandi[a], N.J. Meeuwenoord[b], D.V. Filippov[b], M.Huber*[a]

Department of Physics, Huygens-Kamerlingh Onnes Laboratory, Leiden University, 2300 RA Leiden, The Netherlands

Leiden Institute of Chemistry, Gorlaeus Laboratoria, Leiden University, 2300 RA Leiden, The Netherlands

Table of Contents

Supplementary Figures

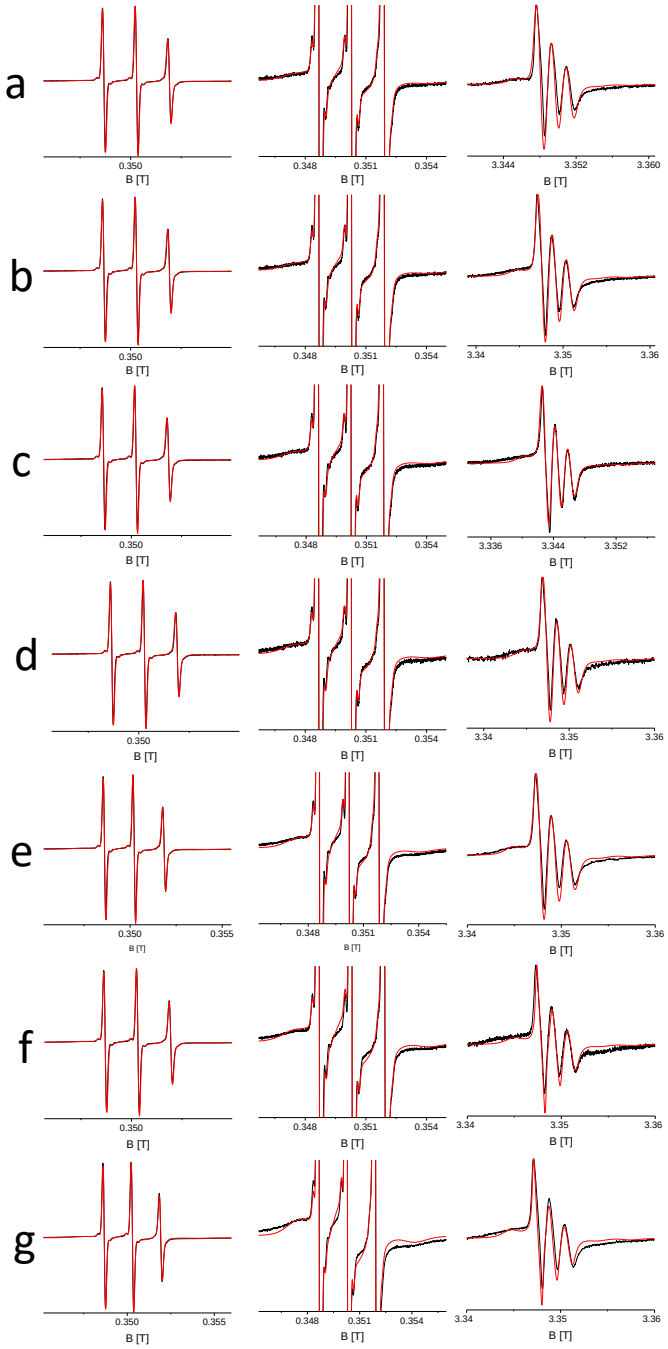

Fig. S1 *Room temperature 9 and 95 GHz EPR spectra of T0EZ for the entire time point series taken during aggregation. Left: 9 GHz EPR, full spectra. Central: 9 GHz EPR spectra, amplitude expanded ten-fold. Right column: 95 GHz spectra. Spectra a) 0 hrs, b) 1 hr, c) 4 hrs, d) 24 hrs, e) 48 hrs, f) 72 hrs, g) 168 hrs. Black: Experimental spectra. Red: Simulated spectra. Remaining experimental conditions and detailed description: See main text.*

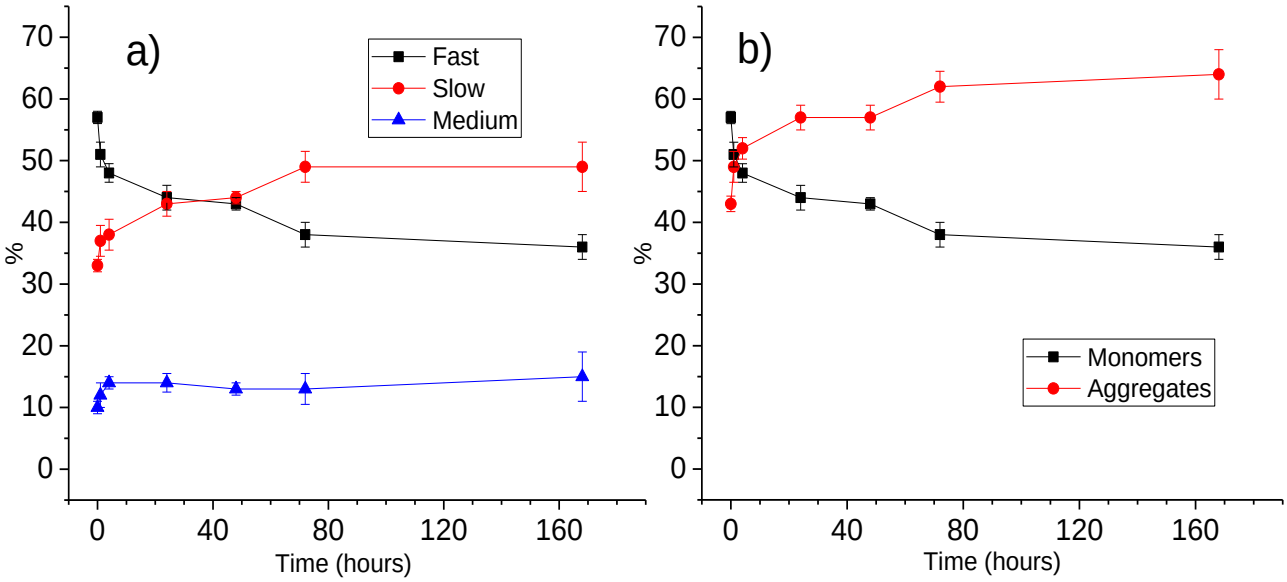

Fig. S2 *a) Amount of the fast, medium and slow components in the EPR spectra of T0EZ as a function of the aggregation time: fast (black), medium (blue) and slow (red). b) From Fig. 4 in the main text: Slow and medium components combined (red). The lines are a guide to the eye.*

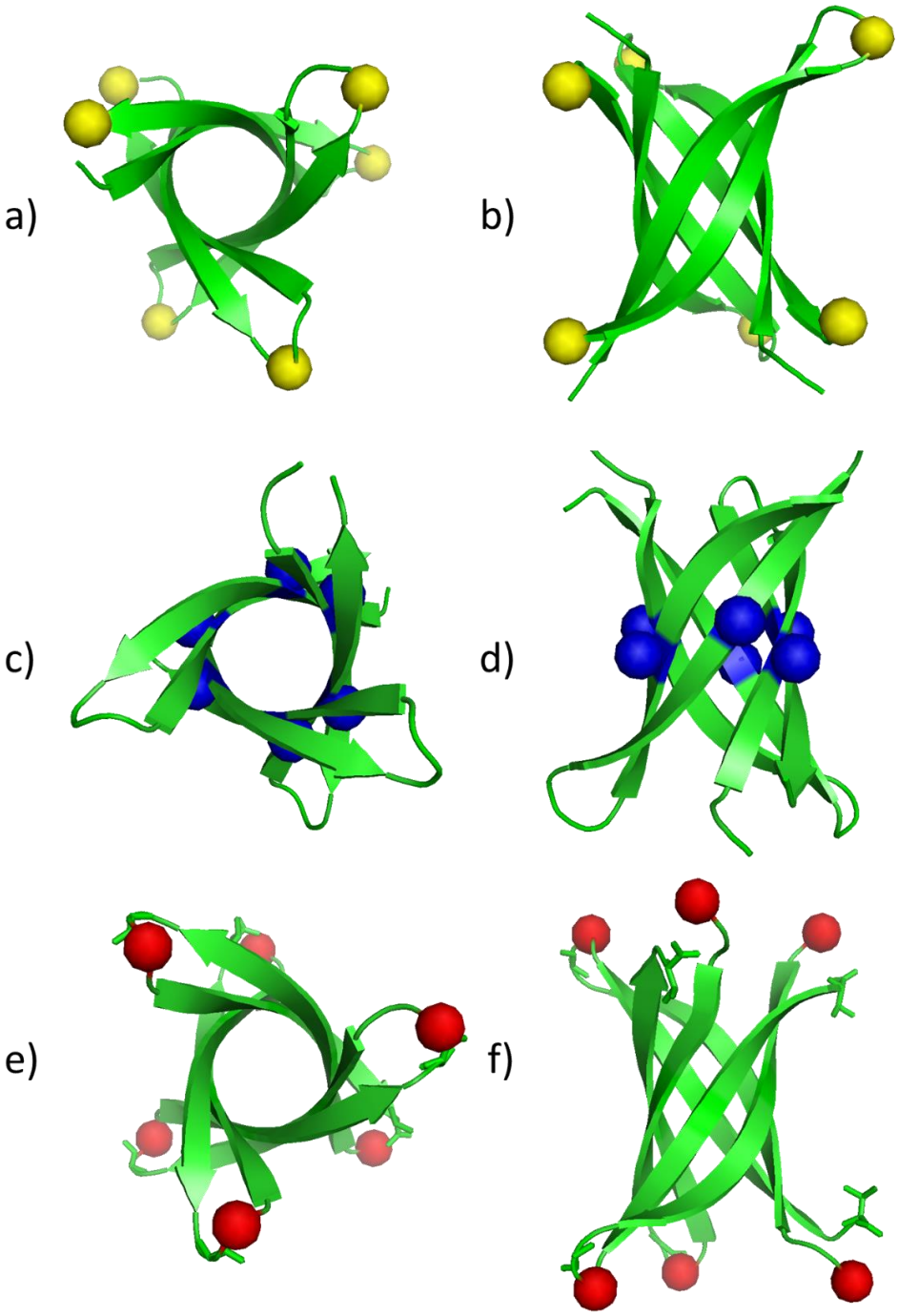

Fig. S3 *Location of TOAC spin label expected for T12EZ, T5EZ and T0EZ, given the structure of the K11V oligomer (PDB 3SGO)*[1]*. a) T12EZ-TOAC: yellow spheres. b) view in a) rotated by 90°. c) T5EZ-TOAC: blue spheres. d) view in c) rotated by 90°. For reference also for T0EZ, the TOAC location is shown: e) T0EZ-TOAC: red spheres. f) view in e) rotated by 90°, see also Fig. 1a) and b).*

Supplementary Materials and Methods

Circular Dichroism

The CD spectra were obtained using a J-815 CD Spectrometer (Jasco Benelux, Utrecht, The Netherlands). The measurements were carried out at room temperature under the conditions of 260 nm - 190 nm wavelength range, continuous scanning mode, a band width and a data pitch of 1 nm each, a speed of 20 nm/min and a total of five accumulations for each measurement. The 40 µL samples for each aggregation time point were diluted ten times in milli-Q water. A 2-mm-path-length cuvette was used for measurements.

Supplementary Data

Circular Dichroism of T0EZ aggregation

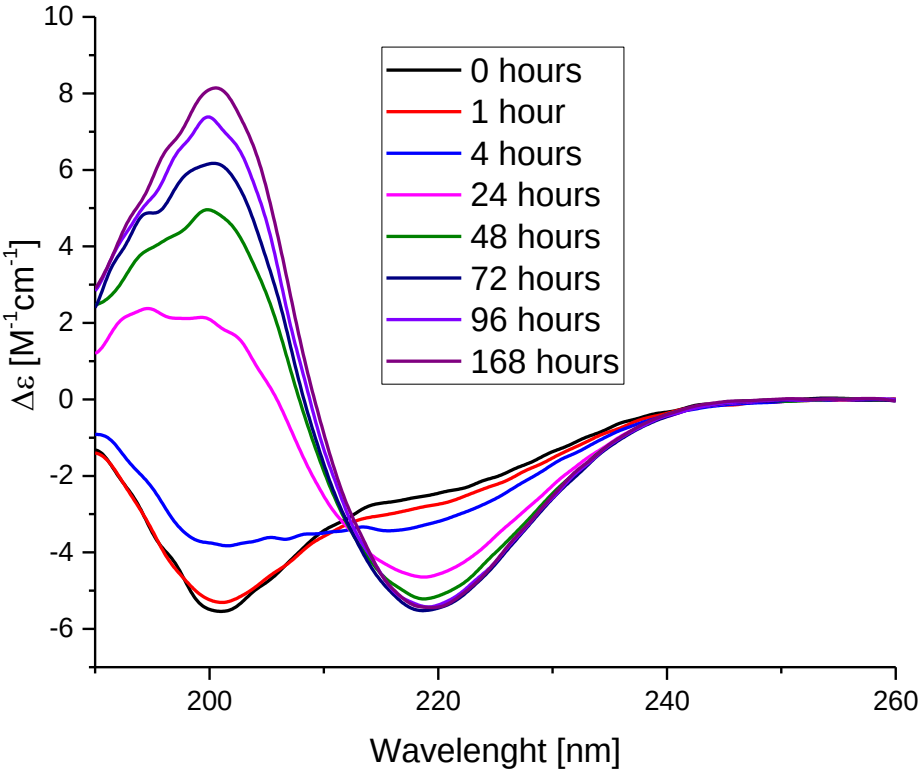

Fig. S4 *Development of the CD spectra of T0EZ measured at different time points of aggregation at room temperature. The spectra have been smoothed by 15 points FFT filter by Origin® for better visualization. At time zero the spectrum (black) presents a lineshape of a random coil structure. After 168 hours the spectrum (wine) shows a lineshape of a β-sheet secondary structure.*

Fig. S4 shows the T0EZ circular dichroism (CD) spectra measured over the time course of aggregation. In Fig. S4 there is a gradual progression of the lineshape from random coil to a β-sheet configuration. The negative feature at 200 nm, characteristic for random coil, becomes positive through time which is a sign of β-sheet structure formation. The negative peak with increasing amplitude around 218 nm is also characteristic of β-sheet. The development suggests an increase of β-sheet character over time, which is expected for β-sheet oligomers.

To obtain the secondary structure composition of the sample according to the CD spectra we use the BeStSel program designed to decompose the CD spectra of proteins. Fig. S5 shows the results for the 190 nm to 260 nm wavelength range. As CD averages the secondary structure per residue over time whereas EPR yields the composition per peptide, a 1 : 1 correspondence of the percentage contribution cannot be expected. Nevertheless, the methods show the same trend: Decay of random coil (CD) and monomer content (EPR) and an increase in β-sheet (CD) and oligomers (EPR). Numerically, random coil and EPR fast fraction agree for the samples up to 20 hours, after that the agreement is better when the random coil and turn fractions from the CD analysis are added. The model of K11V predicts anti-parallel arrangements of the strands in the K11V oligomer, so the parallel β-sheet component in the CD analysis is surprising. As also the attribution of secondary structure elements in CD spectra within BeStSel is not completely established, additional structural information about the species occurring during oligomerization would be needed to clarify this point. Distance measurements by EPR[2–5] could provide this kind of information, however, it is beyond the scope of the present investigation.

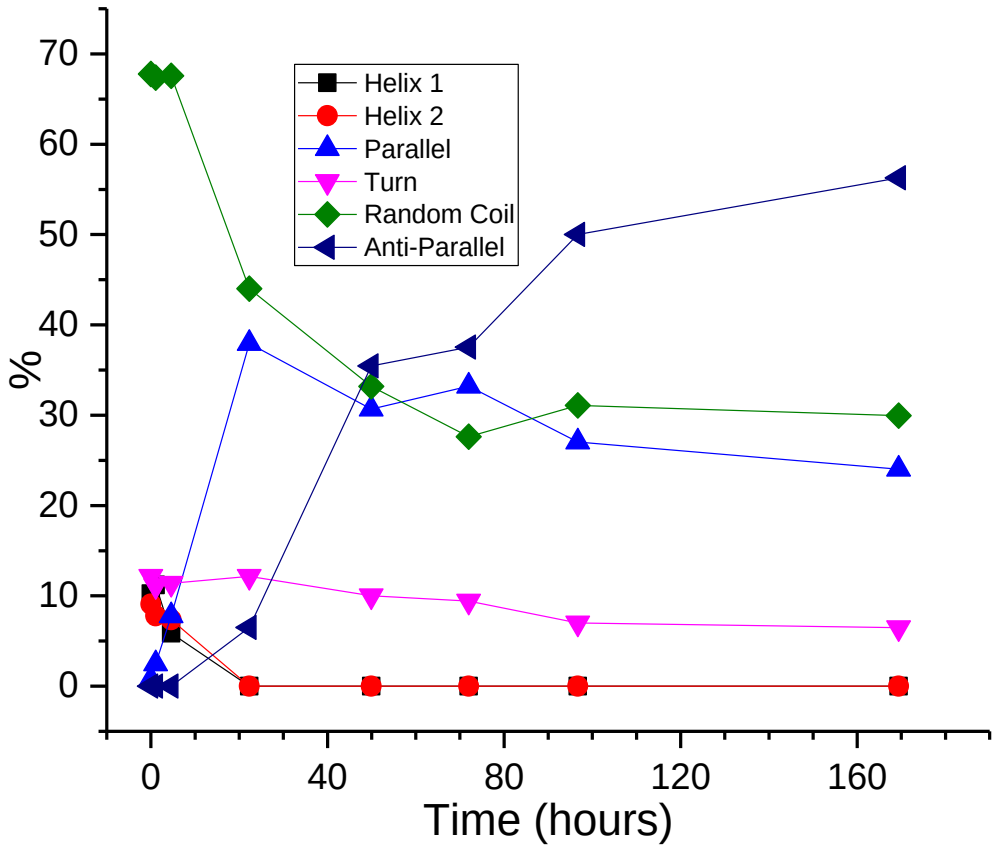

Fig. S5 *Analysis of the CD spectra in Fig. S4 using BeStSel software[6,7], showing the amount of the secondary structures of T0EZ over time derived from the CD spectra. Helix 1 (black) and helix 2 (red) are the different helical conformations. Random coil (green) is considered as mainly being the "Others" component of BeStSel. BeStSel provides three antiparallel β-sheet components, left-twisted (Anti1), relaxed (Anti2) and right twisted (Anti3), which are added up here as Anti-Parallel (navy). For the first 4 hours, when Anti1 and Anti2 were zero, the value of Anti3 (having a basis spectrum similar to that of the disordered structure), was added to the random coil. Parallel (blue) is the parallel β-sheet structure. Turn (pink) is the beta-turn structure. The lines are a guide to the eye.*

Activity of TOAC and diamagnetic dilution

Low spin label activity in peptides results in diamagnetic dilution. Protonation by strong acids (TFA) used during peptide synthesis to cleave the peptide from the resin (see Materials and Methods) is known to reduce and thereby inactivate the nitroxide of TOAC at least partially[8].

Two experiments show that this is also the case for T0EZ: The concentration of the peptide determined from the weight of the lyophilized powder is five times higher than the spin concentration determined by EPR, as described in Materials and Methods, showing that only 20 % of the TOAC is active in the peptide. To confirm that TOAC is inactivated by TFA, a sample of T0EZ in DMSO was incubated for 3 hours by adding 10 % of a solution of NH_3 in water (Sigma-Aldrich 28-30 %). After incubation, the EPR signal had increased by a factor of four, confirming that acid-deactivation by TFA is the most likely origin of low spin concentration of the as-synthesized T0EZ.

While usually undesired, here we use the as-synthesized T0EZ without activation because the low activity of TOAC provides a convenient – and otherwise difficult to realize – way to diamagnetically dilute spins. During aggregation the peptide with a paramagnetic, active TOAC will be incorporated randomly with the inactive peptides into the aggregates, which is referred to as diamagnetic dilution. Diamagnetic dilution increases the spin-spin distance, generating spectra devoid of spin-spin interactions, if (i) the ratio of inactive vs active labels is sufficiently large considering the expected distance and (ii) if the species with active spin labels are randomly distributed in the structure.

$$z = \frac{n!}{(n-p)!\,p!} \cdot a^p \cdot (1-a)^{n-p} \qquad (S1)$$

To estimate if condition (i) is fulfilled, we analyze the spin proximity in the cylindrin hexamer[9]. Eqn. S1 defines which fraction of hexamers *z* contains a given number *p* of active TOAC labels. In Eqn. (S1) *z* is the population of spin-labelled oligomers, *p* is the number of active spin labels in the oligomer, *n* is the number of monomers in the aggregate and *a* is the fraction of active spin labels.

For a *p* of 2 Table S1 shows that 26 % of the hexamers are expected to contain two labeled peptides. In this fraction the distances between the two spin centers is expected to be either 15 Å or 25 Å[1]. This corresponds to a dipolar interaction of 2.45 MHz and 0.53 MHz, i.e. 0.09 mT to 0.02 mT. Such a broadening would be undetectable given the width of the spectral lines, allowing us to neglect any influence of spin-spin interactions in the analysis. A random distribution of active and inactive peptides

(assumption (ii)) is likely as both types of peptides only differ in the protonation state of the nitroxide, so they have almost identical chemical structures

Table S1 *Number of spin-labelled peptides with active nitroxides expected for hexameric oligomers.*

p	*z* %
0	23.0 ± 2.0
1	38.0 ± 3.0
2	26.0 ± 2.0
3	9.8 ± 0.8
4	2.0 ± 0.2
5	0.2 ± 0.1

Simulations of EPR spectra: Quality of the fits

As described in the main text, the overall strategy was to simulate the spectra with a common set of parameters, using the smallest number of components that fit the entire time series, to avoid overfitting the data. Here we discuss this approach in more detail and describe its consequences for the simulations. Three components, the fast, medium and slow, were sufficient. For each individual time point, the 9 and 95 GHz EPR spectra were fitted with the same composition of these three components, finding the optimum that agrees best for both spectra. Relaxing these constraints or introducing other mobility models, such as anisotropic rotation models[10–12], improves the simulation of the individual spectra, but introduces additional parameters that may result in overfitting the spectra. The results of the three-component simulations are displayed in Fig. S1, in which the simulated spectra are shown in red. For aggregation times up to 24 hours, the agreement of simulation and experiment is very good for 9 and 95 GHz spectra, whereas later time-point spectra show some deviation: As a representative for deviations, we discuss the spectra in Fig. S1f): The experimental 95 GHz spectrum has intensity at the low field side of the spectrum (B_0 = 3.340-3.345 T) and the high field side of the spectrum (B_0 = 3.353-3.357 T) that is not covered by the simulation. This spectral intensity would correspond to a very slow/immobilized component in the spectrum that is not compatible with the 9 GHz EPR spectrum. The appearance of such a slow component in the 95 GHz spectra could derive from instrumental effects: The

overall baseline stability in 95 GHz EPR is worse than in 9 GHz, so part of this broad component could be attributed to such instabilities. They would have a stronger impact on the later time spectra, because the amplitude of the narrow, three-line spectrum is less, causing an apparent increase in amplitude of baseline artefacts (note that in Fig. S1 the spectra are amplitude scaled to the narrow component). Secondly, the samples for 95 GHz EPR had to be stored frozen before the measurements, whereas most of the 9 GHz EPR spectra were measured directly after the samples were drawn from the aggregation mixture. It cannot be excluded that freezing affects the sample. We therefore considered this spectral intensity in the 95 GHz EPR spectra as less important and focused more strongly on the 9 GHz EPR spectra of this particular time point. Apparently, for this time point the optimum solution for both 9 and 95 GHz EPR spectra limits the degree of agreement of simulation and experiment that can be reached.

Comparison of τ_r in TOAC versus MTSL-labelled EZ peptides

Table S2 *Experimentally determined rotational correlation times of monomeric EZ peptides from 9 GHz and 95 GHz EPR. MXEZ: construct with MTSL at the same position as the TOAC in TXEZ. Molecular volumes from EPR (V_{EPR}) and molecular weight (V_{MW}) are also given (see main text).*

Peptides	τ_R Monomers [ns]	V_{EPR} [nm^3][a]	V_{MW} [nm^3][b]
T0EZ	0.16 ± 0.004	0.65 ± 0.02	1.78
T5EZ	0.40 ± 0.02	1.61 ± 0.07	1.65
T12EZ	0.31 ± 0.02	1.25 ± 0.06	1.78
M0EZ	0.14 ± 0.01	0.56 ± 0.03	1.89
M5EZ	0.18 ± 0.003	0.73 ± 0.01	1.69
M12EZ	0.15 ± 0.004	0.59 ± 0.02	1.89
K11V			1.47
EZ			1.61

a) From Stokes-Einstein (Eqn. 1).

b) From protein density (ρ = 1.35 g/cm^3) (Eqn. 2).

Table S2 gives the values of τ_r of the monomeric EZ peptides obtained from the simulations of the 9 GHz and 95 GHz EPR spectra. In addition to the values for T0EZ, T5EZ and T12EZ (Table 3 main text) also values for the MTSL-labelled EZ peptides are given. The MTSL-EZ peptides contain the spin-labelled

cysteine at the N-terminus (M0EZ), at position 5 (M5EZ) and at position 12 (M12EZ), for sequences see Table 1 in the main text. All MTSL-constructs have shorter τ_r than the TOAC counterparts, reflecting a higher local mobility of the MTSL label than the TOAC label. The difference in τ_r is largest for T5EZ and M5EZ. The τ_r value for T0EZ is half of that of T12EZ, as discussed in the main text. This shows that the backbone mobility is higher at the N-terminus than at the C-terminus of the EZ peptide. The rotational correlation times of M0EZ and M12EZ are the same within the experimental error, showing that local mobility, i.e. rotation about the single bonds linking the nitroxide to the backbone, masks backbone-mobility differences.

We tested the MTSL-labelled peptides for aggregation the same way as for the TOAC counterparts. The M0EZ peptide aggregated similarly to T0EZ. Similar to T5EZ and T12EZ, also M5EZ and M12EZ failed to aggregate. As MTSL labels do not break β-sheets, this finding shows that the inhibition of aggregation from crowding of the spin labels is more important than β-sheet breaking propensity of the TOAC.

Approximations used in oligomer size estimation

As described in the main text, the Stokes-Einstein relation establishes that τ_r is proportional to the volume of the aggregate and, together with the protein density, it gives an estimate for the number of monomers in the aggregate. Utilizing this approach involves several approximations, the impact of which we describe in the following. Some of these approximations can be tested against the known structure of one of the oligomers expected for the EZ peptides: The hexamer cylindrin[1]. For this oligomer the X-ray structure is known and the rotational correlation times can be calculated from first principles by HYDRONMR[13].

Table S3 *Size of oligomers from different methods and effects of approximations. Number of monomers in oligomer n_i. Rotational correlation times (τ_r) in ns are also given.*

			n_i		
			method (i)		**method (ii)**
EPR component	**τ_r from EPR [ns]**	**τ_r from HYDRONMR [ns]**	**ρ = 1.35 g/cm^3**	**ρ = 1.50 g/cm^3**	
medium	2.00 ± 0.20	5.78[a)]	4.52	5.03	5.81
slow	6.31 ± 0.70	n.a.	14.27	15.88	18.31

a) τ_1 = 4.96 ns; τ_2 = 6.20 ns; τ_3 = 6.16 ns

Influence of protein density on values of n_i (method (i))

The protein density impacts n_i as seen in Table S3, comparing the two columns headed method (i). A value of ρ = 1.35 g/cm^3 (left column) is generally accepted for typical folded proteins (MW > 20 kDa)[14] yielding the parameters that are also given in the main text, however, for proteins with progressively smaller MW, the density is increasing due to a larger relative impact of the hydration shell at lower protein volumes[15]. Thus a larger density (ρ = 1.5 g/cm^3) appears appropriate under some circumstances, and the resulting values are given in the right column[14]. Comparing the two columns, the oligomer sizes differ by 0.5 (medium fraction), resp. 1.5 (slow fraction) monomer units, showing that for the medium fraction the size approaches a pentamer. As the slow EPR fraction suggests a molecular weight of 23 kDa, the higher density does not seem appropriate for that fraction, showing that n_i for that fraction should be closer to a 14-mer than a 16-mer.

Using monomer volume for cylidrin (method (ii))

Method (ii) uses the volume of the monomer derived from the volume of the hexameric oligomer as obtained from x-ray crystallography[1], eqn. (4) main text. It does not require the protein density. It results in a hexamer for the medium and a 18-mer for the slow fraction.

Influence of the spherical approximation on n_i

The Stokes-Einstein relation (Eqn. 1, main text) implies a spherical object. For non-spherical objects the volumes derived from the Stokes-Einstein relation do not reflect the volume of the object accurately, as described here. Also, the lineshape of the EPR spectra can show systematic variations from those of a spherical object, and rather than by a single τ_r, the isotropic τ_r (τ_0), the anisotropic τ_r values τ_1, τ_2 and τ_3 should be used.

The impact of any deviation of the shape of the oligomers from a sphere on the volume is estimated considering the theory of axially symmetric rotational ellipsoids. Axially symmetric rotational ellipsoids are described by the axis system *a, b, c*, where *a* is the semi-axis along the symmetry axis and *b* and *c* are perpendicular to it. For a > b, a prolate, and for a < b, an oblate ellipsoid results. The relation between τ_r and the volume of such particles is described by Perrin et al.[16], Koenig et al.[17] and summarized by Marsh and Horvath[18]. For cylindrin[1], where the radius of the cylinder (11 Å) is equal to the half-height of the cylinder (total height 22 Å), b/a = 1 results and Fig. 1 of Koenig[17] shows that τ_1, the rotation correlation time about the symmetry axis *a,* is 1.4 times larger than τ_r of a sphere of the same volume (τ_0). Along the two equivalent axes $\tau_r \approx \tau_0$. The averaged τ_r for such an ellipsoid could therefore be 1.3 times longer than

that of a sphere. Thus the volume of the cylindrical ellipsoid would be 1.3 smaller than that of a sphere. For the smaller oligomers (medium τ_r fraction from EPR) the number of monomers in the oligomers would reduce from five to four. The effect of other aspect ratios on τ_r can be obtained from Fig. 1 in Koenig[17]. In all cases, the τ_r values of non-spherical objects are larger than those of a sphere of equivalent volume, suggesting a systematic over-estimation of the particle size in the spherical approximation. As the anisotropy of the rotation should be visible in the EPR spectra, EPR experiments at higher field/frequency values would help to determine the degree of anisotropy. Such experiments are beyond the scope of the present study.

Influence of local mobility on oligomer size

If the motion of the nitroxide is faster than that of the oligomer, the oligomer size determined by τ_r would be smaller than the real value, an effect referred to as local mobility of the nitroxide. For proteins labelled conventionally with the MTSL label, Fig 1d, this is a severe problem. The nitroxide TOAC, Fig. 1c, is part of the protein backbone, which will suppress local mobility effects considerably. The τ_r of one of the EZ peptides (T5EZ) matches its volume (see Tab 3, main text) showing that local mobility at the center of the peptide is negligible, also, this τ_r is significantly longer than that of M5EZ, emphasizing that the τ_r of TOAC peptides is more closely correlated with the size of the object than for peptides labelled with MTSL. As described in the main text, the N-terminus of T0EZ must be somewhat flexible, so we cannot exclude that the size of the oligomer is somewhat underestimated. We are not aware of studies that have quantitatively analysed this point, in contrast to the situation for MTSL where extensive studies were performed by the Hubbell group[19–24].

Hydrodynamic simulations by HYDRONMR

For K11V, the structure of one oligomer is known, so the τ_r value for this structure can be calculated by HYDRONMR. The obtained τ_r values give insight into the anisotropy of the rotation and absolute τ_r values for the hexamer. In Tab. S3 these values are given: the anisotropy is relatively small and agrees well with an axially symmetric prolate object. The absolute isotropic τ_r value is longer than calculated by methods (i) and (ii). Clearly , HYDRONMR provides a more realistic representation of the structure of the oligomer and of the hydration layer. The empirically derived protein densities take hydration into account, however, without considering the surface details of the protein and methods (i) and (ii) imply spherical approximation. The impact of the respective approaches for oligomers of the type observed here are difficult to assess. We observe that the τ_r of the hexamer cylindrin from HYDRONMR is

significantly longer than that of the medium fraction. There are two possible interpretations: Either, the medium fraction is due to a smaller oligomer than the cylindrin, or the faster τ_r value observed experimentally is due to local mobility.

Final assessment

As far as the effect of the approximations of the approaches described can be quantified, the errors introduced are 1-1.5 monomer units per oligomer (e.g. method (i)). Some approximations lead to systematic deviations: Deviation of the oligomer from a sphere causes the oligomer size to be overestimated, local mobility causes the opposite effect and one could hope for some cancellation of errors. Conservatively, an estimate of 2-3 monomers units results for the absolute number of monomers in the oligomers, however, as several factors causing these uncertainties may be similar for some or all oligomers, relative sizes are more reliable and qualitative size distinctions can be made. In the main text, Discussion section, specialized experiments based on pulsed EPR and other techniques are described that can determine accurate oligomer sizes, however, most of these cannot be applied in situ. The present approach provides the overview of the entire aggregation process and can identify states of interest, e.g. how many distinct oligomer states there are, and what the relative sizes of oligomers are. Once established, these states can be investigated more quantitatively by the methods referred above

Can single monomer resolution of oligomer size be attained?

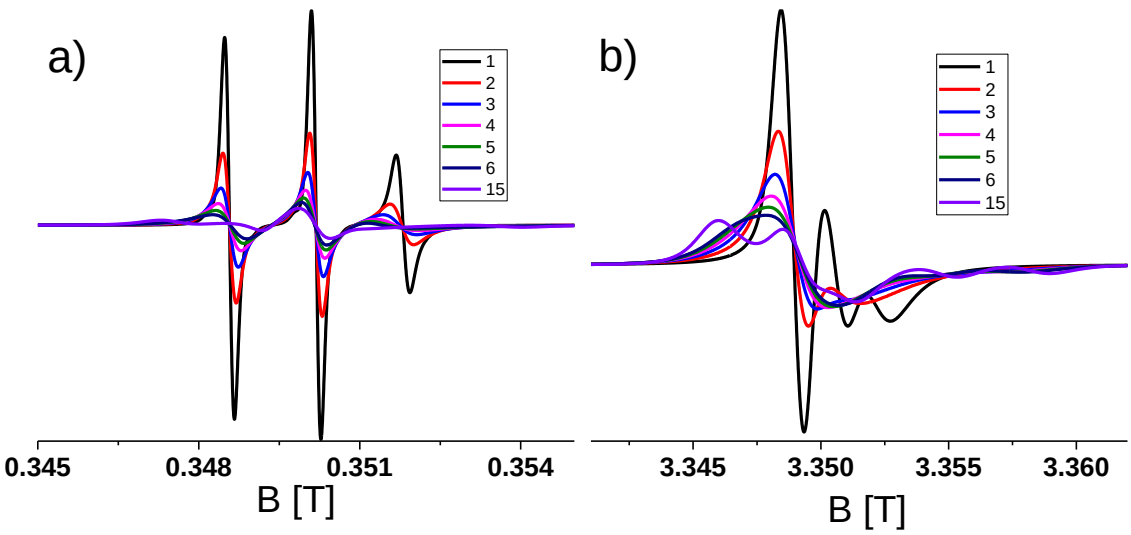

Fig. S6 *Simulations of EPR spectra of T0EZ for the expected volumes of different sized oligomers, one monomer at a time. The* τ_r *values were calculated based on the* V_{MW} *using the same parameters as for the simulations of the experimental spectra (see Material and Methods in the main text). a) Simulations of 9 GHZ spectra of a molecule with rotational correlation times ranging from 1.8 ns (black) to 26.7 ns (purple). b) Simulations of 95 GHZ spectra for the same rotational correlation times.*

Fig. S6 shows the 9 GHz and 95 GHz EPR spectra expected for oligomers of different sizes in single-monomer increments. Sizes range from 1 to 15 mer aggregates. Peptide volume used: V_{MW} of T0EZ. Especially in the 95 GHz EPR spectra, the differentiating power of the method is high: Monomers are clearly set off from dimers, and up to hexamers individual species can clearly be distinguished in the low- and high-field region of the spectra. Similarly, resolving oligomers from hepta- to 15 mers should be possible, but it is not shown here for clarity.

1 A. Laganowsky, C. Liu, M. R. Sawaya, J. P. Whitelegge, J. Park, M. Zhao, A. Pensalfini, A. B. Soriaga, M. Landau, P. K. Teng, et al., *Science* 2012, **335**, 1228–31.

2 N. Alexander, A. Al-Mestarihi, M. Bortolus, H. Mchaourab, J. Meiler, *Structure* 2008, **16**, 181–195.

3 C. C. Jao, B. G. Hegde, J. Chen, I. S. Haworth, R. Langen, *Proc. Natl. Acad. Sci.* 2008, **105**, 19666–19671.

4 P. G. Fajer, *J. Phys. Condens. Matter* 2005, **17**, S1459–S1469.

5 G. Jeschke, *Annu. Rev. Phys. Chem.* 2012, **63**, 419–446.

6 A. Micsonai, F. Wien, É. Bulyáki, J. Kun, É. Moussong, Y.-H. Lee, Y. Goto, M. Réfrégiers, J. Kardos, *Nucleic Acids Res.* 2018, **46**, W315–W322.

7 A. Micsonai, F. Wien, L. Kernya, Y.-H. Lee, Y. Goto, M. Réfrégiers, J. Kardos, *Proc. Natl. Acad. Sci.* 2015, **112**, E3095-E3103.

8 R. Marchetto, S. Schreier, C. R. Nakaie, *J. Am. Chem. Soc.* 1993, **115**, 11042–11043.

9 A. Laganowsky, C. Liu, M. R. Sawaya, J. P. Whitelegge, J. Park, M. Zhao, A. Pensalfini, A. B. Soriaga, M. Landau, P. K. Teng, et al., *Science (80-.).* 2012, **335**, 1228–1231.

10 E. Meirovitch, Z. Liang, J. H. Freed, *Solid State Nucl. Magn. Reson.* 2018, **89**, 35–44.

11 E. Meirovitch, Z. Liang, J. H. Freed, *J. Phys. Chem. B* 2015, **119**, 14022–14032.

12 D. E. Budil, S. Lee, S. Saxena, J. H. Freed, *J. Magn. Reson. Ser. A* 1996, **120**, 155–189.

13 J. García de la Torre, M. . Huertas, B. Carrasco, *J. Magn. Reson.* 2000, **147**, 138–146.

14 H. Fischer, I. Polikarpov, A. F. Craievich, *Protein Sci.* 2004, **13**, 2825–2828.

15 L. R. Murphy, N. Matubayasi, V. A. Payne, R. M. Levy, *Fold. Des.* 2005, **3**, 105–118.

16 F. Perrin, *J. Phys. le Radium* 1936, **7**, 1–11.

17 S. H. Koenig, *Biopolymers* 1975, **14**, 2421–2423.

18 D. Marsh, Horváth L.I., *Advanced EPR: Applications in Biology and Biochemistry*, Elsevier, 2012.

19 C. J. López, M. R. Fleissner, Z. Guo, A. K. Kusnetzow, W. L. Hubbell, *Protein Sci.* 2009, **18**, 1637–1652.

20 L. Columbus, T. Kálai, J. Jekö, K. Hideg, W. L. Hubbell, *Biochemistry* 2001, **40**, 3828–3846.

21 Z. Zhang, M. R. Fleissner, D. S. Tipikin, Z. Liang, J. K. Moscicki, K. A. Earle, W. L. Hubbell, J. H. Freed, *J. Phys. Chem. B* 2010, **114**, 5503–5521.

22 R. Langen, K. J. Oh, D. Cascio, W. L. Hubbell, *Biochemistry* 2000, **39**, 8396–8405.

23 M. R. Fleissner, D. Cascio, W. L. Hubbell, *Protein Sci.* 2009, **18**, 893–908.

24 W. L. Hubbell, D. S. Cafiso, C. Altenbach, *Nat. Struct. Biol.* 2000, **7**, 735–739.